

Direct bandgap optical transitions in Si nanocrystals

A. A. Prokofiev¹, A. S. Moskalenko^{2,1}, I. N. Yassievich¹

¹*Ioffe Physico-Technical Institute, Polytechnicheskaya 26, 194021 Saint-Petersburg, Russia*

²*Institut für Physik, Martin-Luther-Universität Halle-Wittenberg, Germany*

W. D. A. M. de Boer³, D. Timmerman³, H. Zhang⁴, W. J. Buma⁴ and T. Gregorkiewicz³

³*Van der Waals-Zeeman Institute, University of Amsterdam,
Valckenierstraat 65, NL-1018 XE Amsterdam, The Netherlands*

⁴*Van 't Hoff Institute for Molecular Sciences, University of Amsterdam
Nieuwe Achtergracht 129, NL-1018 WS Amsterdam, The Netherlands*

(Dated: October 29, 2018)

The effect of quantum confinement on the direct bandgap of spherical Si nanocrystals has been modelled theoretically. We conclude that the energy of the direct bandgap at the Γ -point decreases with size reduction: quantum confinement enhances radiative recombination across the direct bandgap and introduces its “red” shift for smaller grains. We postulate to identify the frequently reported efficient blue emission (F -band) from Si nanocrystals with this zero-phonon recombination. In a dedicated experiment, we confirm the “red” shift of the F -band, supporting the proposed identification.

PACS numbers: 73.22.Dj, 78.67.Bf, 78.67.Hc

Crystalline silicon, which dominates electronic and photovoltaic industry, has notoriously inferior optical properties for light emission. This follows from its energy structure which features an indirect bandgap, with the absolute minimum of the conduction band being very much displaced — $\Delta k = 0.85 \times (2\pi/a)$ along the $[100]$ -direction — from the Γ -point, where the maximum of the valence band is positioned. The direct bandgap energy at the Γ -point amounts to $E_g^{\text{dir}} = 3.32$ eV in bulk Si. On the way towards photonic and opto-electronic applications of silicon, possibly the most promising route is offered by space-confinement-induced changes of energy structure. Following the pioneering paper of Canham on porous Si [1], investigations of various forms of nanostructured Si have been undertaken. In particular, very interesting results were obtained for Si nanocrystals (NCs) where strong effects of quantum confinement have been observed for grain sizes comparable to or smaller than the effective Bohr radius of 4.3 nm — e.g. see Ref. [2] for an extensive review. It has been shown that while the energy structure in Si NCs retains its indirect character, quantum confinement leads to relaxation of the momentum conservation requirement, thus making zero-phonon optical interband transitions possible. Nevertheless, phonon-assisted radiative transitions dominate for nanocrystal sizes down to 2 nm [3]. Therefore, the emission from Si-NCs has two characteristic features: for smaller grains, the spectrum shifts to the blue and its intensity increases. In the literature, this widely tuneable and rather efficient emission due to ground state electron-hole recombination is usually referred to as the “slow” band (S -band). It has attracted a lot of attention and prospects of Si-NCs-based laser have been discussed [4].

In addition to the S -band whose origin is well established, optical investigations of Si-NCs revealed also another emission band at higher energies. This “blue”

band is characterized by much faster decay dynamics (hence the name F -band), ranging from pico- to nanoseconds. A similar emission band has also been reported for porous Si [5]. Its origin is currently debated both experimentally and theoretically [6–8]. Usually, it is postulated to arise due to radiative recombination of electrons localized at oxygen-related states at Si/SiO₂ interface [9, 10]. This interpretation has been recently challenged by Valenta [11], who presented evidence that the F -band should rather be identified with transitions related to the NCs themselves. Emission bands in the visible have also been reported in colloidal Si-NCs [12, 13] and postulated to arise due to direct transitions in view of their short lifetime.

In this paper, we consider effect of quantum confinement on the conduction band at the Γ -point in spherically symmetric Si-NCs. According to the presented theoretical model, quantum confinement applied to the conduction band states in the vicinity of the Γ -point, creates two series of states with energies higher and lower than the energy of the conduction band at the Γ -point in bulk Si (3.32 eV), forming a gap between them. We attribute the lower series of states as the origin of direct optical transitions responsible for the F -band. In that interpretation, the F -band is microscopically identified as arising due to zero-phonon recombination of “hot” electrons from the Γ -point of the conduction band. We discuss that as the confinement gets stronger with decreasing the NC size and the direct band gap shrinks, the “red” shift of the F -band appears. We confirm this theoretical conclusion by dedicated experimental evidence concerning spectral dependence and dynamics of the F -band in a dense solid state dispersion of Si-NCs in a SiO₂ matrix. We demonstrate that the proposed microscopic identification of the F -band is consistent with this experimental data as well as with the available literature.

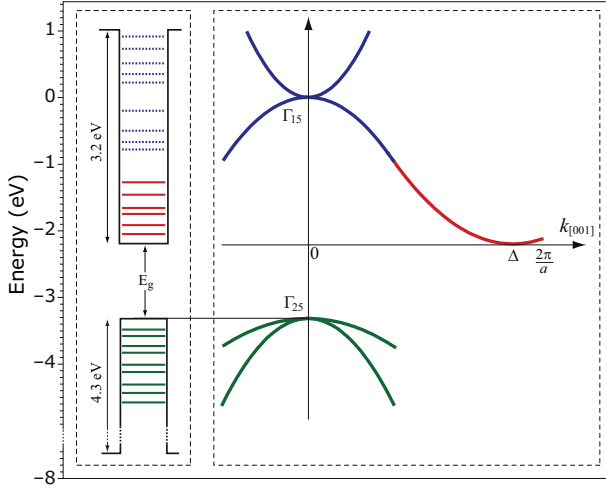


FIG. 1: Fig. 1. Right panel: schematical representation of the dispersion relations for the conduction and the valence bands of bulk silicon along the [001] direction [14]. Left panel: quantum potentials in real space and confinement energy levels for electrons and holes. Our model attributes the lower quantum levels (solid lines) of electrons to the states originating from Δ -valley of the conduction band, and the higher excited ones (dotted lines) to the states of the Γ -point.

The scheme of the lowest conduction band in bulk silicon (based on detailed calculations from Ref. [14]) is shown in the right panel of Fig. 1. In the center of Brillouin zone its states are of Γ_{15} symmetry, thus being 3-fold degenerate (without spin taken into account), and they are related to two subbands, one of which (the “heavy” one) has negative effective mass. It is the negative effective mass that leads to emerging of space-confinement levels below the band edge and therefore to decrease of the threshold of direct optical transitions.

Counting energy of electrons from the Γ_{15} -point, one can write a generalization of the Luttinger Hamiltonian in spherical approximation:

$$\hat{H} = (A + 2B) \frac{\hat{\mathbf{p}}^2}{m_0} - 3B \frac{(\hat{\mathbf{p}} \cdot \hat{\mathbf{J}})^2}{m_0}, \quad (1)$$

where m_0 is the free electron mass, $\hat{\mathbf{p}}$ is the momentum operator, and $\hat{\mathbf{J}}$ is the unitary angular momentum operator acting in the space of Bloch amplitudes. The coefficients A and B , related to the effective mass values, are extracted from the results of Ref. [14] by weightening the band parameters obtained for different directions: $A = 0.4A_{001} + 0.6A_{111} = 0.58$, $B = 0.4B_{001} + 0.6B_{111} = -0.85$. Such values correspond to positive energy and “light” effective mass of $m_{el} = 0.35 m_0$ for doubly degenerate subband and negative energy and “heavy” effective mass of $m_{eh} = -0.45 m_0$ for the other nondegenerate subband. In a spherical quantum dot Hamiltonian (1) results in three types of states [16], which are the eigenfunctions of the square \hat{F}^2 of the full angular momentum operator $\hat{\mathbf{F}} = \hat{\mathbf{J}} + \hat{\mathbf{L}}$ (operator $\hat{\mathbf{L}} = -i\mathbf{r} \times \nabla$ acts on the

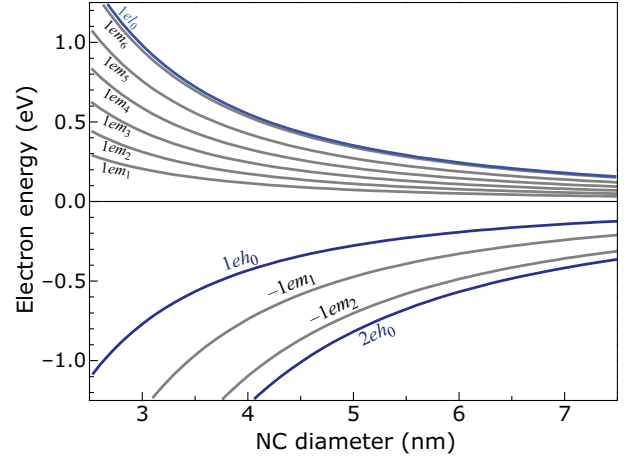


FIG. 2: Fig. 2. Energy levels of electrons at the Γ -point in spherical Si-NC as a function of its diameter. According to Fig. 1, zero energy corresponds to the energy of bulk Si conduction band at the Γ -point.

envelope parts of the wave functions only) and its projection \hat{F}_z . They are

- i) “heavy” states Neh_0 with $F = 0$,
- ii) “light” states Nel_F ($F \geq 1$),
- iii) “mixed” states $\pm Nem_F$ ($F \geq 1$),

where N is the main quantum number and the subscript shows the value of F .

To investigate qualitatively the effect of confinement on the energy spectrum, we calculated the space-quantization levels of electrons in the vicinity of the Γ_{15} -point assuming for them infinitely high energy barriers at the NC boundary. The resulting energy spectrum as a function of NC size is shown in Fig. 2. One can see that the spectrum is split: “light” states have positive energy, “heavy” — negative, and “mixed” ones have both positive and negative energy levels. The most important feature of the resulting spectrum is that the energy gap is formed and the absolute values of negative energy levels are rising with decreasing diameter of NCs. We should remark that the appearance of such a gap was predicted in Ref. [15] with help of rudimentary pseudopotential calculations. The quantization energies of holes are rising as well [16], but it does not change the trend, and the transition energy does decrease for given transition with decreasing the size.

The rate of direct spontaneous optical recombination is given by [17]:

$$\tau_{\text{rad}}^{-1} = \frac{4}{3} \alpha^3 \omega_{\text{out}} |M|^2 \mathcal{F}^2, \quad (2)$$

where $\alpha = \hbar/(m_0 a_0 c) \approx 1/137$ is the fine structure constant, a_0 is Bohr radius, c is the speed of light, $\hbar\omega$ is the transition energy, $\mathcal{F} = 3n_{\text{out}}^2/(n_{\text{in}}^2 + 2n_{\text{out}}^2)$ is the local field factor [17], with n_{in} and n_{out} being refraction indexes of media inside and outside the NC respectively (for the NCs under consideration $\mathcal{F} \approx 0.42$). The dimen-

TABLE I: Factors I_R^2 for several interband transitions, as well as their energies for two NC sizes: 3 and 7 nm.

Transition	$d = 3 \text{ nm}$		$d = 7 \text{ nm}$	
	I_R^2	$\hbar\omega$	I_R^2	$\hbar\omega$
$1eh_0 \rightarrow 1hm_2$	1.185	2.95 eV	1.277	3.28 eV
$-1em_1 \rightarrow 1hh_2$	0.099	2.53 eV	0.130	3.23 eV
$-1em_1 \rightarrow 1hm_1$	0.016	2.17 eV	0.002	3.13 eV
$2eh_0 \rightarrow 1hm_2$	0.077	1.45 eV	0.047	3.01 eV

sionless matrix element M in (2) is defined by:

$$|M|^2 = \frac{a_0^2}{\hbar^2} \frac{1}{N_e} \frac{1}{N_h} \sum_{M_e, M_h} \sum_{\alpha=x,y,z} \left| \sum_{v,c} \int (\psi_v^{M_h})^* \psi_c^{M_e} d^3r \langle u_v | \hat{p}_\alpha | u_c \rangle \right|^2, \quad (3)$$

where $N_e = 2F_e + 1$ and $N_h = 2F_h + 1$ are the degeneracy factors of the electron and hole states respectively, and $\psi_c^{M_e}$ ($\psi_v^{M_h}$) are the envelope parts of the electron (hole) wave function $\Psi_{F_e M_e} = \sum_c \psi_c^{M_e} u_c$ ($\Psi_{F_h M_h} = \sum_v \psi_v^{M_h} u_v$). The Bloch amplitudes basis u_c is chosen in the form of spherical components $u_0 = Z_c$, $u_\pm = \mp \sqrt{1/2}(X_c \pm iY_c)$, where $X_c = x$, $Y_c = y$, and $Z_c = z$ are the functions of the Γ_{15} representation. It should be noted that the consideration of hole states in [16] has also been produced with the Bloch amplitude basis u_v in the form of spherical components but using functions $X_v = yz$, $Y_v = xz$, and $Z_v = xy$ of the $\Gamma_{25'}$ representation. The difference in the Bloch amplitude bases makes the direct optical transitions between electron and hole states permitted.

The value of the matrix element of momentum between the Bloch amplitudes of the valence and the conduction bands p_{cv} allowed by the selection rules can be written in the form: $p_{cv}^2 = |\langle X_c | \hat{p}_y | Z_v \rangle|^2 = |\langle Y_c | \hat{p}_z | X_v \rangle|^2 = |\langle Z_c | \hat{p}_x | Y_v \rangle|^2 = Q^2 \hbar^2 / a_0^2$, where $Q = 1.07$ [14]. And the total matrix element (3) is $|M|^2 = Q^2 I_R^2$, where I_R is a combination of overlap integrals of the envelope functions. There are also selection rules for overlap integrals of envelope functions in Eq. (3) arising due to the spherical symmetry of both electron and hole states. E.g., in our consideration, radiative transitions from “heavy” electron states Neh_0 can only go into the valence band states of “mixed” type, characterized by $F = 2$: Nhm_2 . These rules should not be strict for real NCs, which are not perfectly spherical, and transitions disabled by our model are still possible, but we expect them to be much weaker.

Finally, for the estimation of radiative recombination rate one can use:

$$\tau_{\text{rad}}^{-1} = 1.0 \times 10^8 \left(\frac{\hbar\omega}{3 \text{ eV}} \right) I_R^2, \text{ s}^{-1}. \quad (4)$$

The values of I_R^2 for the radiative transitions with the smallest energies are listed in Table I. For the most ef-

fective transition $Neh_0 \rightarrow Nhm_2$ the radiative life time is of the order of 10 ns. We propose that the emissions observed as the F -band arise due to transitions in Table I. Table I also illustrates that the energy range of possible transitions increases with decrease of NC diameter.

The radiative emission under consideration can be produced only by “hot” confined electrons. Thus the rate of nonradiative relaxation of these electrons is a key issue for the observation of this emission. We have studied transitions between levels in the vicinity of the Γ_{15} -point taking place due to multiple emission of optical phonons and emission/absorption of one promoting acoustic longitudinal phonon. The probability of such a transition is given by $W = \tau_{\text{ac}}^{-1} J_p(T, S)$, where τ_{ac} is the time determined by the interaction with an acoustic phonon, T is temperature, S is the Huang-Rhys factor, and $J_p(T, S)$ is the factor specific for multiphonon transitions which for $S \ll 1$ and kT less than the optical phonon energy $\hbar\omega \approx 60 \text{ meV}$ can be well approximated by $S^p/p!$, where p is the number of emitted optical phonons [18]. We have calculated the Huang-Rhys factor following Ref. [18] and using Bir-Pikus Hamiltonian $H_{\text{e-ph}}^{\text{opt}}(\mathbf{u}^{\text{opt}}) = \frac{2}{\sqrt{3}} \frac{d_0}{a} (u_x^{\text{opt}} \{J_y J_z\} + u_y^{\text{opt}} \{J_z J_x\} + u_z^{\text{opt}} \{J_x J_y\})$ for the interaction with optical phonons, where $2\{J_\alpha J_\beta\} \equiv J_\alpha J_\beta + J_\beta J_\alpha$, a is the lattice constant, $d_0 = -16.9 \text{ eV}$ [19] is the interaction constant, and \mathbf{u}^{opt} is the relative atomic displacement induced by the optical phonon mode. In result we have $S = 0.13/d^3$ for $1eh_0 \rightarrow -1em_1$ transition, $S = 0.04/d^3$ for $-1em_1 \rightarrow -1em_2$, and $S = 0.22/d^3$ for $-1em_2 \rightarrow 2eh_0$, where the NC diameter d should be taken in nm. Further we have calculated τ_{ac}^{-1} and then W taking into account the energy difference which is not compensated by the optical phonons and using the interaction Hamiltonian $H_{\text{e-ph}}^{\text{ac}} = a_c \nabla \mathbf{u}^{\text{ac}}$, where $a_c = -10 \text{ eV}$ [19] and \mathbf{u}^{ac} is the atomic displacement induced by the acoustic phonon mode. The highest transition rates are of the order of 10^9 s^{-1} for the largest NCs considered here. They decrease rapidly with the NC size. One can notice that for transitions $1eh_0 \rightarrow -1em_1$ and $-1em_1 \rightarrow -1em_2$ several optical phonons are needed even for large NCs with extremely small Huang-Rhys factors (see Fig. 2). In case of small NCs more phonons are required and Huang-Rhys factors are still small so that the phonon-induced relaxation is suppressed. The state $-1em_2$ can decay quicker than the other states due to smaller energy spacing to the lower neighboring state but it anyway does not contribute to the considered radiative transitions (see Table I).

The proposed theoretical identification of the F -band is directly supported by photoluminescence (PL) experiments performed on Si-NCs embedded in a SiO_2 matrix. Two different samples were used, both prepared by radio frequency co-sputtering and subsequent annealing, resulting in an average NC diameter of 3 nm (sample A) and 5.5 nm (sample B), with a small size distribution — see, e.g. Refs. [20, 21] for more details on sample preparation and measuring techniques. Figure 3 shows the results obtained for both samples in two differently

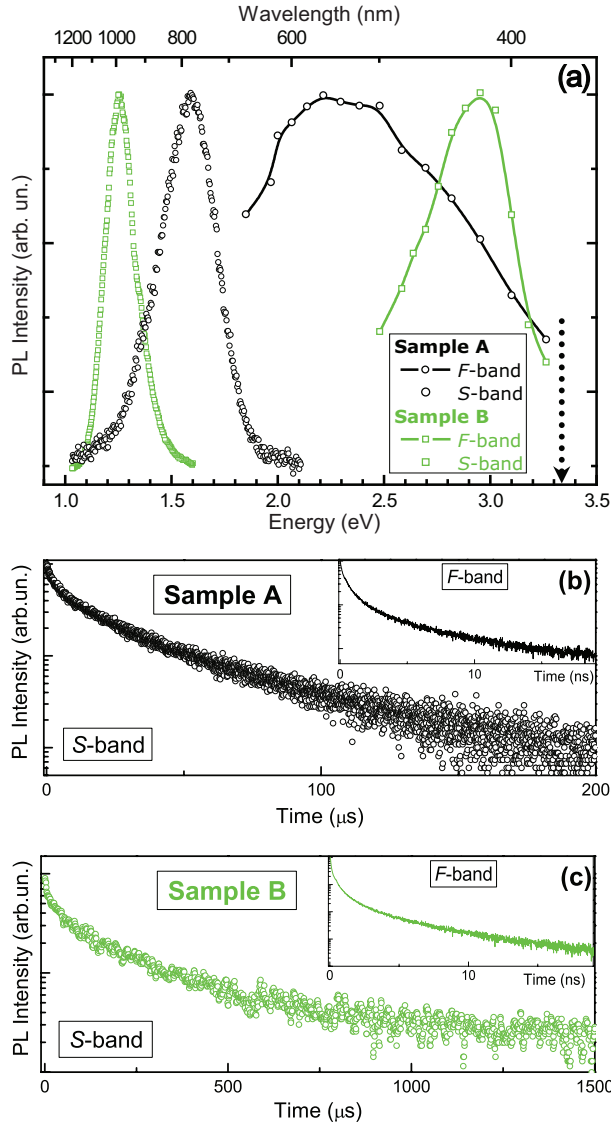


FIG. 3: (a) S (scattered symbols) and F (solid line + symbols) PL bands for sample A (circles) and sample B (squares). Dashed arrow indicates the position of direct bandgap recombination as experimentally measured for bulk Si [24]. (b,c) PL dynamics for sample A (figure b) and sample B (figure c): S -band decay is displayed in main panels. The kinetics were fitted with a stretched exponential: $I_{PL} = I_0 e^{-(t/\tau)^\beta}$, with $\beta = 0.8$ [25]. The relevant time constants are $\tau_A^S \approx 20 \mu s$ for sample A and $\tau_B^S \approx 510 \mu s$ for sample B. The inset shows dynamics of the F -band in a time window of 50 ns taken at the maximum intensity values of 2.5 eV and 3 eV for samples A and B, respectively.

conducted PL experiments. With the steady-state technique, the slow (microsecond range) time-integrated PL signal was monitored. This is dominated by the low-energy S -band (indicated in Fig. 3(a) with \circ) and, as a result of quantum confinement, shows the well-known

shift towards higher photon energies for smaller NCs. The spectral profile of the F -band has been obtained by taking the initial amplitude of the ps-resolved dynamics and is illustrated in Fig. 3(a)(—). As can be seen, the F -band shows a red shift upon size decrease — an effect opposite to the blue shift characteristic for the S -band. This behavior is in agreement with the presently calculated shift towards lower energies of the electron energy levels at the Γ -point — see Fig. 2 — and the consequent reduction of the direct bandgap value. We note that the linewidth of the F -band clearly increases for smaller NCs, as indeed expected due to quantum confinement. The time-resolved PL measurements have been obtained in a time-correlated single photon counting experiment. Figs 3(b) and 3(c) illustrate dynamics of S and F PL bands for both samples. The decay time of the S -band (main panels, nanosecond resolution) is of an order of $\sim 10^2 \mu s$, i.e. similar to the estimated radiative recombination time of excitons in Si-NCs [16, 22]. It is somewhat faster for smaller NCs (sample A in respect to B), reflecting the increased radiative recombination rate [23]. The decay dynamics of the F -band (insets, picosecond resolution) is characterized by a time constant of $\tau_F \approx 500$ ps, similar for both samples. Finally, we point out that the fact that the F -band can be monitored using (ps-resolution) time-resolved PL experiments, implies that an upper limit can be set to the ratio of the non-radiative transition rate to the radiative recombination rate of $(\tau_{nonrad}^F)^{-1} \div (\tau_{rad}^F)^{-1} \leq 10^2$. On that basis, the radiative recombination time for the F -band can be estimated as $\tau_{rad}^F \leq 50$ ns.

We conclude that the characteristic features following from the proposed theoretical model for the direct Γ -point phonon-less recombinations — (i) decrease of the energy and (ii) linewidth broadening for smaller NC sizes are experimentally confirmed for the F -band emission from Si-NCs. Also the radiative lifetime of the F -band estimated from the measured PL dynamics agrees with the calculated values. These additional new experimental evidence taken together with the information on F -band available in the literature, agree very well with the proposed identification of this fast emission with radiative recombination across the direct bandgap of Si, whose energy has been lowered in Si-NCs due to quantum confinement.

Further research, currently on the way, will elucidate details of the direct bandgap tuning in Si-NCs.

This work has been supported by Stichting voor de Technologische Wetenschappen (STW), Nederlandse Organisatie voor Wetenschappelijk Onderzoek (NWO), and Russian Foundation for Basic Research (RFBR) as well as grants of the Russian President. The samples on which the experimental results were conducted, have been developed in cooperation with Dr. M. Fujii from Kobe University.

-
- [1] L. Canham, Appl. Phys. Lett. **57**, 1046 (1990).
 - [2] D. Kovalev, H. Heckler, G. Polisski, and F. Koch, Phys. Stat. Sol. **215**, 871 (1999).
 - [3] D. Kovalev *et al.*, Phys. Rev. Lett. **81**, 2803 (1998).
 - [4] L. Pavesi *et al.*, Nature (London) **408**, 440 (2000).
 - [5] L. Tsybeskov, Ju. V. Vandyshov, and P. M. Fauchet, Phys. Rev. B **49**, 7821 (1994).
 - [6] F. Trojáněk, K. Neudert, M. Bittner, and P. Malý, Phys. Rev. B **72**, 075365 (2005).
 - [7] V. Kuntermann *et al.*, Phys. Rev. B **77**, 115343 (2008).
 - [8] Y. Chao, A. Houlton *et al.*, Appl. Phys. Lett. **88**, 263119 (2006).
 - [9] M. V. Wolkin, J. Jorne, P. M. Fauchet, G. Allan, and C. Delerue, Phys. Rev. Lett. **82**, 197 (1999).
 - [10] C. Delerue, G. Allan and M. Lannoo, Phys. Rev. B **48**, 11024 (1993).
 - [11] J. Valenta *et al.*, New J. Phys. **10**, 073022 (2008).
 - [12] J. P. Wilcoxon and G. A. Samara, Appl. Phys. Lett. **74**, 3164 (1999).
 - [13] D. S. English, L. E. Pell, Y. Zhonghua, P. F. Barbara, and B. A. Korgel, Nanolett. **2**, 681 (2002).
 - [14] M. Cardona, F. H. Pollak, Phys. Rev. **142**, 530 (1966).
 - [15] M. V. Rama Krishna and R. A. Friesner, J. Chem. Phys. **96**, 873 (1992).
 - [16] A. S. Moskalenko, J. Berakdar, A. A. Prokofiev, I. N. Yassievich, Phys. Rev. B **76**, 085427 (2007).
 - [17] C. Delerue, M. Lannoo, *Nanostructures: Theory and Modelling* (Springer-Verlag, Berlin, 2004).
 - [18] S. V. Goupalov, Phys. Rev. B **72**, 073301 (2005).
 - [19] A. Blacha, H. Presting, and M. Cardona, phys. stat. sol. (b) **126**, 11 (1984).
 - [20] Y. Kanzawa *et al.*, Solid Stat. Commun. **102**, 533 (1997).
 - [21] D. Timmerman *et al.*, Nature Phot. **2**, 105 (2008).
 - [22] K. Watanabe, M. Fujii, and S. Hayashi, J. Appl. Phys. **90**, 4761 (2001).
 - [23] M. Sykora *et al.*, Phys. Rev. Lett. **100**, 067401 (2008).
 - [24] P. Schmidt, R. Berndt, and M. I. Vexler, Phys. Rev. Lett. **99**, 246103 (2007).
 - [25] J. Linnros, N. Lalic, A. Galeckas, and V. Grivickas, J. Appl. Phys. **86**, 6128 (1999).